07

Modeling of processes of irradiation of Cr/4H-SiC structures with high-energy Ar ions

© M.A. Chumak, E.V. Kalinina, V.V. Zabrodskii

Ioffe Institute, St. Petersburg, Russia
e-mail: equilibrium2027@yandex.ru

Received October 7, 2024
Revised January 27, 2025
Accepted January 30, 2025

A comprehensive mathematical modeling of the processes of radiation defect formation under 4H-SiC irradiation with Ar ions was performed. Ultraviolet photodetectors based on Cr/4H-SiC Schottky barriers with a charge carrier concentration of $3 \cdot 10^{15}\,\mathrm{cm}^{-3}$ in a $5\,\mu$m thick CVD layer were irradiated 7 times with Ar ions with a fluence of $1 \cdot 10^{10}\,\mathrm{cm}^{-2}$ (total fluence - $7 \cdot 10^{10}\,\mathrm{cm}^{-2}$) with an energy of 53 MeV. Based on the results of measuring the external quantum efficiency of the photodetectors at different fluences of irradiation with Ar ions and modeling the irradiation processes in SRIM/TRIM, it is shown in what range of values the concentration of radiation defects should be under irradiation for a noticeable decrease in the quantum efficiency to occur up to its complete degradation at limiting fluences. For the specified concentration of charge carriers, the limiting fluence of Ar ions leading to complete degradation of Cr/4H-SiC photodetectors was determined experimentally for the first time. As a result of modeling, the ratio of silicon and carbon vacancies by the depth of the Ar ion stopping distance was determined for the first time. Key words: silicon carbide, Ar ions, irradiation, SRIM/TRIM, depth profiles, external quantum efficiency.

Keywords: Silicon carbide, Ar ions, irradiation, SRIM/TRIM, depth profiles, external quantum efficiency.

DOI: 10.61011/TP.2025.06.61379.356-24

Introduction

Semiconductor devices for power, high-frequency and nuclear applications, engineering of radiation detectors require the use of high-temperature, radiation-resistant materials capable of operating in aggressive media. The most widely used commercial semiconductor is silicon carbide of 4H polytype with its unique electrophysical characteristics. The large band gap (3.23 eV), high thermal conductivity (at copper level), extremely low leakage currents ($10-25\,\mathrm{A} \cdot \mathrm{cm}^{-2}$), high threshold energy of defect formation allow operation at high temperatures (up to 900 °C) and at increased radiation levels [1–5]. The radiation resistance of 4H-SiC was proved when irradiated with electrons, protons, neutrons, powerful X-ray pulses, as well as ions in a wide range of their masses and energies [6,7]. Of particular interest is heavy ion irradiation which simulates structural damage caused by nuclear fission fragments [8,9]. It should be stressed that there are no publications covering the impact of limiting fluences occurring after photodetectors irradiation with Ar ions, leading to complete degradation of the characteristics of SiC-based photodetectors.

Mathematical modeling in TRIM software implementing Monte Carlo method is used to predict the results of radiation defect formation in semiconductors irradiated with flows of charged particles [10]. Mathematical modeling also makes it possible to predict and analyze the characteristics of new devices prior to their production, thereby significantly reducing their development costs. In addition, it makes it possible to visualize many physical phenomena and processes in the volume of a semiconductor, which are quite difficult to measure and estimate when working with a real crystal [11–13]. When 4H-SiC was irradiated with protons and various ions, mathematical modeling was partially used to determine energy losses, calculate the profile of interstitial particles, calculate the number of vacancies and the parameters of ion-induced displacements [6,9,14–20].

The purpose of this work is to determine the limiting fluence of Ar ions during a step-by-step irradiation of Cr/4H-SiC detector structures with energy 53 MeV by $1 \cdot 10^{10}\,\mathrm{cm}^{-2}$ fluence (total fluence — $7 \cdot 10^{10}\,\mathrm{cm}^{-2}$), and to conduct complex modeling of radiation defects formation in irradiated structures, compare the modeling results with changes in the spectra of external quantum efficiency of Cr/4H-SiC photodetectors.

1. Materials and methods

1.1. Description of a real modeling object

Irradiation was simulated for 4H-SiC samples with Cr Schottky barriers designed for detection of the ultraviolet (UV) radiation within the wavelengths 40–400 nm [21]. On 4H-SiC substrates with a thickness of $400\,\mu$m with a concentration of non-compensated donors$N_d - N_a = (1-3) \cdot 10^{18}\,\mathrm{cm}^{-3}$ by method of chemical

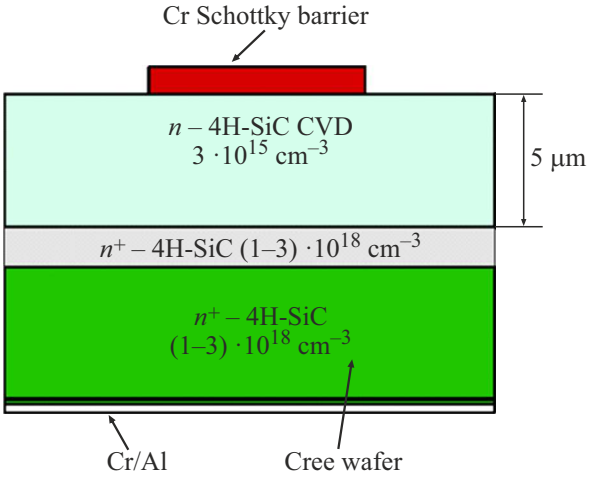

Figure 1. Cross-section of 4*H*-SiC detector with Cr Schottky barrier.

vacuum deposition (CVD) first, only thin highly doped buffer layer $< 1\,\mu$m thick was buildup, after that 4*H*-SiC layer with a thickness of $5\,\mu$m with a concentration of $N_d - N_a = 3 \cdot 10^{15}\,\text{cm}^{-3}$ was formed (Fig. 1). Cr/Al base contacts and Cr Schottky barriers were formed by thermal vacuum sputtering using various spraying technologies. Cr Schottky barriers were sputtered through the masks with a diameter of 2–8 mm and thickness of 20 nm.

The samples were irradiated with Ar ions from the side of Cr-Schottky barriers step by step 7 times using $1 \cdot 10^{10}\,\text{cm}^{-2}$ fluence with an energy of 53 MeV at a temperature of 25 °C on the cyclotron at Ioffe Physical-Technical Institute. Taking into account the characteristics of cyclotron, it can be argued that heating of samples during implantation with Ar ions is excluded. The fluence was determined by the total charge of Ar ion beam applied to the irradiated target. Since SiC has a cumulative effect, the total fluence after sevenfold irradiation was $7 \cdot 10^{10}\,\text{cm}^{-2}$. The uniformity of density of radiation defects formed on the surface of the samples during implantation with Ar ions was not worse than 7,%.

The spectra of external quantum efficiency of Cr/4*H*-SiC UV photodetectors were measured by comparison using a monochromator based on spectrophotometer SF-16. The source of UV radiation in the wavelength range 200–400 nm was a deuterium discharge lamp DDS-30. The currents were recorded using Keithley picoammeter 6485, the dark currents of Cr/4*H*-SiC photodetectors did not exceed 10^{-13} A.

1.2. Description of modeling method in SRIM/TRIM

Using TRIM software, the depth of penetration of Ar ions into the structure 4*H*-SiC was estimated at an energy of 53 MeV, energy losses of incoming ions and phonon generation, the total number of defects and the number of vacancies formed Si and C. In addition, using TRIM software, the interaction of 4*H*-SiC target atoms with implanted ions were considered both in the epitaxial CVD layer with a thickness of $5\,\mu$m and in the substrate until the ions completely stop at irradiation fluences in the range of $1 \cdot 10^{10} - 7 \cdot 10^{10}\,\text{cm}^{-2}$. In this case, the calculation of binary collisions was used, taking into account Ziegler ion-ion analysis [10]. This is a widely used program in the field of ion beam analysis, which makes it possible to study any target composition, provided that correct properties of the irradiated structure are entered. Using this code, the concentration of vacancies created by the action of Ar ion beam on 4*H*-SiC was estimated in a wide range of their energies. According to TRIM, with the energy of Ar ions of 53 MeV the ions stopping distance was $\sim 10\,\mu$m, i.e. they started to decelerate in the substrate. The layer of Cr with a thickness of 20 nm had no effect on the defects formation in SiC when the ions energy was 53 MeV.

For a more accurate determination of the vacancy concentration, a detailed calculation with a cascade mode of complete damage was performed. 4*H*-SiC structure was selected as a material of the target. For the correct calculation of vacancies in the target the monolayer collisions were calculated [10]. The flux of incident ions can be calculated from the beam current, and the fluence is related to the irradiation time.

2. Results and discussion

The characteristics calculated by TRIM program for 4*H*-SiC material and modeling of Ar ion irradiation process are presented in the table, taking into account the generally accepted values of these parameters at a density of 4*H*-SiC equal to 3.21 g/cm^3.

Fig. 2, *a* illustrates the calculated cascade collisions of Ar ions with the atoms of 4*H*-SiC target to a depth of $12\,\mu$m. The scattering of Ar ions after they had been introduced into the target was no more than $2.5\,\mu$m. With an energy of 53 MeV the total depth of Ar ions penetration into 4*H*-SiC until the full stop didn't exceed $10\,\mu$m. The distribution

Parameters of modeling of SiC irradiation with Ar ions

Energy Ar, MeV	53	
Fluence, cm^{-2}	$1 \cdot 10^{10} - 7 \cdot 10^{10}$	
Number of iterations	10^5	
Thickness of target, μm	12	
Density of SiC target, g/cm^3	3.21	
Atoms	Si	C
Stoichiometric composition	0.5	0.5
Lattice bond energy, eV	3	2
Bond energy of atoms on the surface, eV	7.41	4.47
Displacement energy, eV	28	15

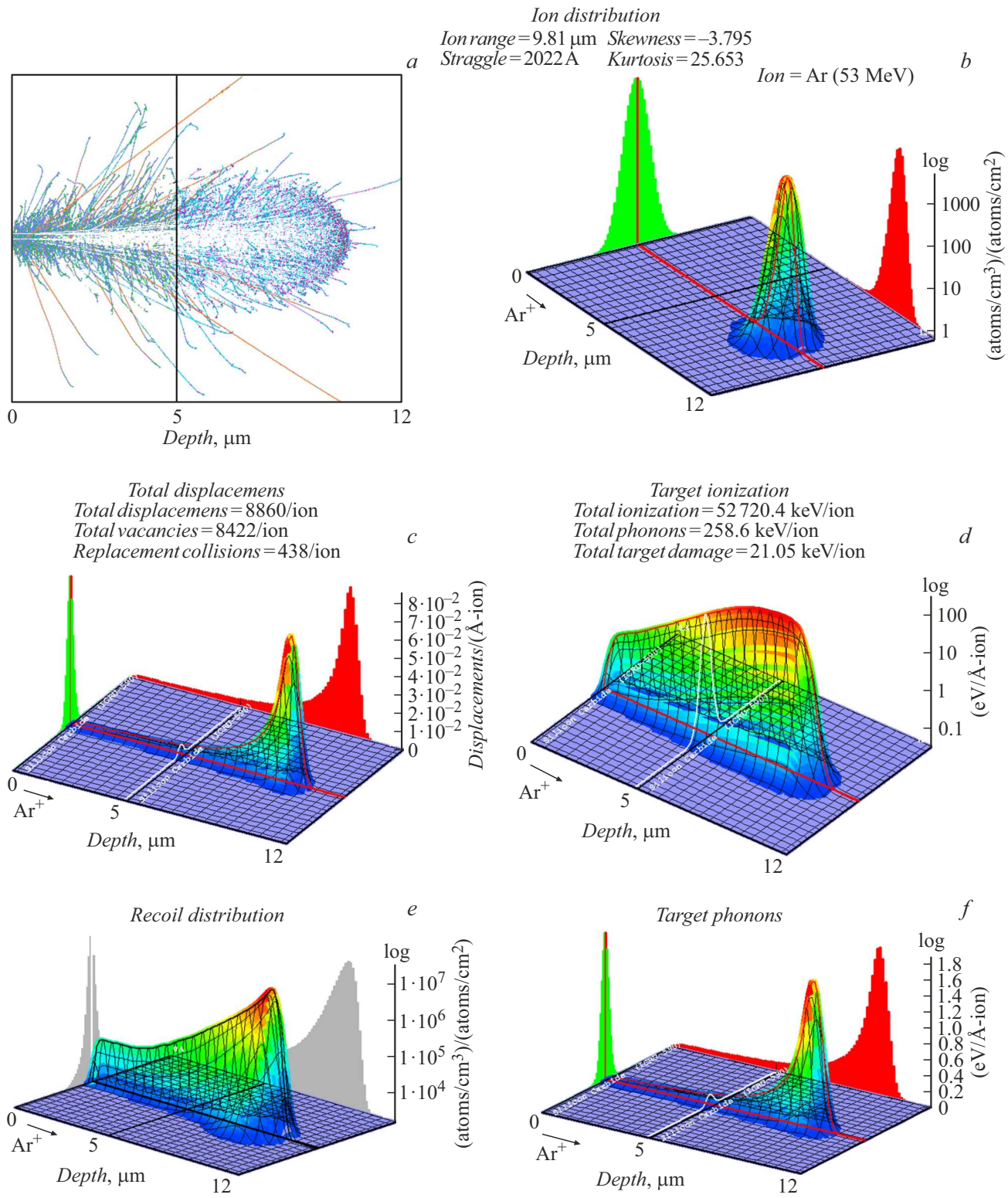

Figure 2. Calculated characteristics obtained during modeling of irradiation of 4*H*-SiC structure with $N_d - N_a = 3 \cdot 10^{15}\,\mathrm{cm}^{-3}$ by Ar ions with an energy of 53 MeV: *a* — displacement cascades formed by Ar ions after 4*H*-SiC irradiation; *b* — profile of distribution of implanted Ar ions in 4*H*-SiC; *c* — distribution of total displacements; *d* — target ionization losses; *e* — distribution of the nocked-on atoms; *f* — generation of phonons.

of Ar ions concentrations in 4*H*-SiC structure demonstrated that their highest concentration was observed at a depth of 9.83 μm (Fig. 2, *b*).

The distribution of collision events over the depth of the simulated structure is shown on a two-dimensional graph (Fig. 2, *c*). The peak of collision events occurred at a depth

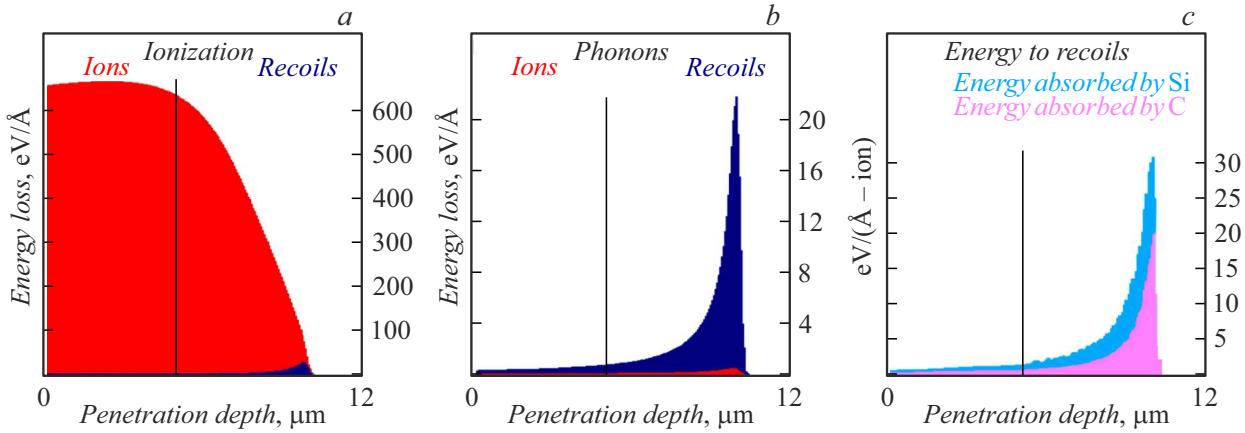

Figure 3. Results of modeling of 4*H*-SiC structure with $N_d - N_a = 3 \cdot 10^{15}\,\mathrm{cm}^{-3}$ irradiation by Ar ions with an energy of 53 MeV and fluence $1 \cdot 10^{10}\,\mathrm{cm}^{-2}$: *a* — ionization losses of target, *b* — generation of phonons, *c* — energy of Ar ions absorbed by Si and C atoms.

of about 9.83 μm at an ion energy of 53 MeV for the target 4*H*-SiC, which is consistent with the distribution of Ar ions concentration (Fig. 2, *b*). The total number of displacements was 8860/ion. The number of Si and C atomic vacancies that was included in the total number of displacements was defined as 8422/ion. Meanwhile, the number of displaced atoms during ion irradiation was 438/ion.

It is calculated that the total energy transferred to damage the target per ion is 21.05 keV/ion. The main ones are ionization losses during the passage of Ar ions in 4*H*-SiC to a complete stop (Fig. 2, *d*). The intensity of distribution of the relative magnitude of ion ionization energy losses in 4*H*-SiC varies depending on the depth of penetration of Ar ions. Full energy transferred to ionization of 4*H*-SiC made 52720.4 keV/ion. Fig. 2, *e* illustrates in detail the distribution of the knocked-on atoms of 4*H*-SiC target. The phonons were distributed across the depth of 4*H*-SiC structure in eV/(Å-ion) units as shown in Fig. 2, *f*. Phonons are described as volumetric lattice vibrations of atoms and molecules. In the case when the transferred energy does not exceed the displacement energy necessary to remove an atom from its lattice by a sufficient distance, it will return to its initial state and emit a phonon. If the energy exceeds the displacement energy, then the atom does not return to its initial state and phonon emission is not observed. Full energy transferred for generation of phonons in 4*H*-SiC target was 258.6 keV/ion. According to calculations, the largest number of phonons is observed at the end of the stopping distance of Ar ions at a depth of $\sim 10\,\mu$m.

Ionization losses, phonon generation, and the energy of Ar ions absorbed by Si and C atoms upon irradiation of 4*H*-SiC by Ar ions with an energy of 53 MeV are shown in Fig. 3, *a*. The data obtained are consistent with the values shown in Figure 2. By the end of the stopping distance of Ar ions ($\sim 10\,\mu$m) the ionization losses in 4*H*-SiC are diminished especially when Ar ions pass the CVD-layer (5 μm) and enter the substrate where they are actively decelerated. The loss of energy for the formation of phonons and the energy absorbed by Si and C atoms, on the contrary, increase sharply (Fig. 3, *b, c*).

The changes in defects concentration in 4*H*-SiC structure with the depth of Ar ions stopping for fluence $1 \cdot 10^{10}\,\mathrm{cm}^{-2}$ are given in Fig. 4, *a*. In addition, the figure shows the profiles of Si and C vacancy concentrations, their total number, and the number of displaced atoms. All profiles of the concentration distribution of all types of defects were approximated by the Pearson function IV. From this it follows that for 4*H*-SiC structure the highest number of defects with a concentration of $8 \cdot 10^{17}\,\mathrm{atom/cm}^3$ is expected at a depth of 9.83 μm when irradiated by Ar ions of this energy.

The concentration of defects in 4*H*-SiC structure in CVD-layer at a depth of 5 μm when irradiated by Ar ions with a fluence $1 \cdot 10^{10}\,\mathrm{cm}^{-2}$ as obtained from the calculations makes about $2.5 \cdot 10^{16}\,\mathrm{cm}^{-2}$ (Fig. 4, *b*). The calculated total defects concentration in the range of fluences of Ar ion irradiation $1 \cdot 10^{10} - 7 \cdot 10^{10}\,\mathrm{cm}^{-2}$ at a depth of the CVD layer 5 μm is in the range $2.6 \cdot 10^{16} - 1.8 \cdot 10^{17}\,\mathrm{atom/cm}^3$ (Fig. 4, *c*).

The calculation results also showed that for the indicated irradiation of 4*H*-SiC with Ar ions, S has the largest number of the nocked-on atoms, since they absorb most of the energy coming from the ions compared to C atoms. This is due to the difference in the masses and sizes of Si atoms (radius 0.24 nm, mass 28.0855 a.m.u.) and C atoms (radius 0.154 nm, mass 12.0107 a.m.u.). It should be noted that the ratio of Si and C vacancies concentrations across the depth of the stopping distance of Ar ions in 4*H*-SiC ($\sim 10\,\mu$m) is non-linear and decreases from 2.42 to 2.19 (Fig. 4, *d*). The growth of C vacancy concentrations occurs faster than the growth of Si vacancies, which is associated with the secondary formation of radiation defects in the displacement cascades [19].

The calculated total defect concentration for Ar $1 \cdot 10^{10} - 7 \cdot 10^{10}\,\mathrm{cm}^{-2}$ ion irradiation fluences was shown

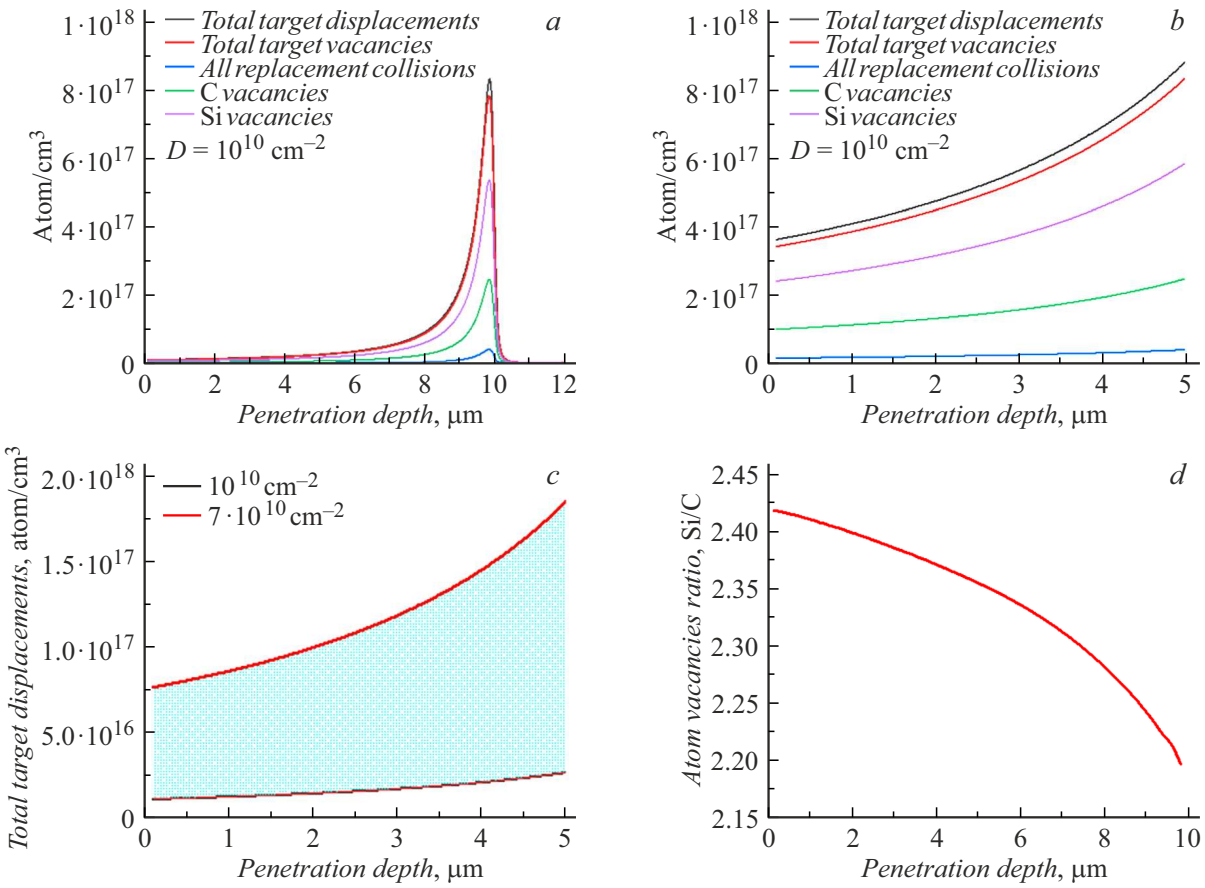

Figure 4. Results of modeling of 4*H*-SiC structure having doping level $N_d - N_a = 3 \cdot 10^{15}\,\text{cm}^{-3}$ irradiated by Ar ions with an energy of 53 MeV: *a, b* — distribution of various defects depending on Ar ions penetration depth when 4*H*-SiC is irradiated with the fluence $1 \cdot 10^{10}\,\text{cm}^{-2}$; *c* — total displacements of 4*H*-SiC in CVD-layer with a thickness of5 μm under irradiation fluences within the range $1 \cdot 10^{10} - 7 \cdot 10^{10}\,\text{cm}^{-2}$; *d* — ratio of concentrations of Si and C vacancies depending on the depth of penetration of Ar ions ($\sim 10\,\mu$m).

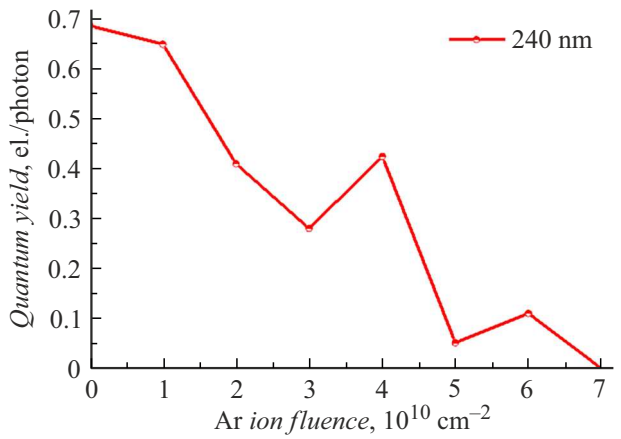

Figure 5. The quantum efficiency of Cr/4*H*-SiC detector with a doping level of $N_d - N_a = 3 \cdot 10^{15}\,\text{cm}^{-3}$ in CVD-layer for UV radiation with the wavelength of 240 nm versus irradiation fluences with Ar ions.

in the results of the quantum efficiency of Cr/4*H*-SiC photodetectors with a concentration of $N_d - N_a = 3 \cdot 10^{15}\,\text{cm}^{-3}$ in the CVD layer. The quantum efficiency decreased from 0.7 electron/photon for an unirradiated sample to 0.01 electron/photon when irradiating the photodetector with fluence $7 \cdot 10^{10}\,\text{cm}^{-2}$ (Fig. 5). For Cr/4*H*-SiC photodetector with the concentration of $N_d - N_a = 3 \cdot 10^{15}\,\text{cm}^{-3}$ in CVD-layer the fluence of Ar ions equal $7 \cdot 10^{10}\,\text{cm}^{-2}$ turned out to be fatal which resulted in worsened quality of the detector. The graph in Fig.5 is shown when irradiated with ultraviolet radiation with a wavelength of 240 nm (direct transition).

Thus, according to calculations and experimental data, in order for the quantum efficiency of a SiC-based photodetector to decrease, the concentration of radiation defects in the near-surface area of the device, where ultraviolet radiation is absorbed, shall stay within $2.6 \cdot 10^{16} - 1.8 \cdot 10^{17}\,\text{atom/cm}^3$. Also, the obtained profile of the concentration of radiation defects for SiC at the limiting fluences of Ar ions, equal to $5 \cdot 10^{10}\,\text{cm}^{-2}$, showed that complete degradation of the characteristics of photocathodes based on 4*H*-SiC occurs when the defect concentration was in the range $5.2 \cdot 10^{16} - 1.8 \cdot 10^{17}\,\text{atom/cm}^3$.

Conclusion

Based on the results of numerical modeling of Cr/4*H*-SiC structures irradiation with high-energy Ar ions, the following may be concluded:

1) when 4*H*-SiC is irradiated with Ar ions with an energy of 53 MeV the ions stopping distance until the full stop is no more than 10 μm for $1-7 \cdot 10^{10}$ cm^2 fluences;

2) the total concentration of radiation defects calculated in the range of radiation fluences $1 \cdot 10^{10}-7 \cdot 10^{10}$ cm^{-2} is within the range $2.6 \cdot 10^{16}-1.8 \cdot 10^{17}$ atom/cm^3;

3) higher concentration of the radiation-induced defects with implantation of Ar ions from $2.6 \cdot 10^{16}$ to $1.8 \cdot 10^{17}$ atom/cm^3 results in lower external quantum efficiency of Cr/4*H*-SiC photodetector;

4) the limiting fluence $7 \cdot 10^{10}$ cm^{-2} was experimentally found when implanted with Ar ions with an energy of 53 MeV resulting in full degradation of Cr/4*H*-SiC photodetector with a concentration of $N_d-N_a = 3 \cdot 10^{15}$ cm^{-3} in CVD-layer;

5) the ratio of Si and C vacancy concentrations over the depth of the stopping distance of Ar ions in 4*H*-SiC epitaxial layer is nonlinear and varies in the range of 2.42–2.19, which is associated with the secondary formation of radiation defects in the displacement cascades.

Conflict of interest

The authors declare that they have no conflict of interest.

Funding

E.V. Kalinina expresses thanks to the Russian Science Foundation for the partial financial support (project № 22-12-00003). M.A. Chumak expresses thanks to the state assignment (project № FFUG-2024-0044) for the partial support of research.

References

[1] J.R. O'Connor, J.R. Smiltens. Semiconductors, **1**, 388 (1960).
[2] J.A. Powell, P.G. Neudeck, L.G. Matus, J.B. Petit. Symp. Proc., **242**, 495 (1992).
[3] O. Kordina, J.P. Bergman, A. Henry, E. Janzen, S. Savage, J. Andre, K. Bergman. Appl. Phys. Lett., **67** (11), 1561 (1995). https://doi.org/10.1063/1.114734
[4] W.J. Choyke, G. Pensl. Mrs Bull., **22** (3), 25 (1997). https://doi.org/10.1557/S0883769400032723
[5] Y. Zhang, W.J. Weber, W. Jiang, A. Hallén, G. Possnert. J. Appl. Phys., **91** (10), 6388 (2002). https://doi.org/10.1063/1.1469204
[6] P.A. Persson, L. Hultman, M.S. Janson, A. Hallén, R. Yakimova, D. Panknin, W. Skorupa. J. Appl. Phys., **92** (5), 2501 (2002). https://doi.org/10.1063/1.1499749
[7] A.Y. Nikiforov, P.K. Skorobogatov, D.V. Boychenko, V.S. Figurov, V.V. Luchinin, E.V. Kalinina. RADECS-2003, **527**–**528**, 1473 (2003).
[8] I. Lhermitte-Sebire, J.L. Chermant, M. Levalois, E. Paumier, J. Vicens. Radiation Effects and Defects in Solids, **126** (1–4), 173 (1993). https://doi.org/10.1080/10420159308219702
[9] W.J. Weber, L.M. Wang, N.Yu. Nucl. Instruments and Methods in Physics Research Section B: Beam Interactions with Materials and Atoms, **116** (1–4), 322 (1996). https://doi.org/10.1016/0168-583X(96)00066-3
[10] J. Ziegler. SRIM code. http://www.srim.org. Last access: January 17th (2022).
[11] P.P. Panchenko, A.A. Malakhov, S.B. Rybalka, A.V. Rad'kov. J. Radio Electron., **8**, 1684 (2016).
[12] V.V. Muravyov, V.N. Mishenka. BGUIR Reports, **104** (2), 53 (2007) (in Russian).
[13] E.A. Kulchenkov, S.B. Rybalka, A.A. Demidov, A.Yu. Drakin. Appl. Mathem. Phys., **52** (1), 33 (2020). https://doi.org/10.18413/2687-0959-2020-52-1-33-40
[14] A.I. Mikhaylov, A.V. Afanasiev, V.A. Ilyin, V.V. Luchinin, S.A. Reshanov, M. Krieger, A. Schöner, T. Sledziewski. Semiconductors, **48** (12), 1581 (2014). https://doi.org/10.1134/S1063782614120148
[15] E.V. Kalinina, G.F. Kholuyanov, G.A. Onushkin, D.V. Davydov, A.M. Strel'chuk, A.O. Konstantinov, A. Hallén, A.Yu. Nikiforov, V.A. Skuratov, K. Havancsak. Semiconductors, **38**, 1187 (2004). https://doi.org/10.1134/1.1808826
[16] S.J. Zinkle, J.W. Jones, V.A. Skuratov. MRS Symp. Proceed., **650**, R3.19.1 (2000). https://doi.org/10.1557/PROC-650-R3.19
[17] P. Kumar, M. Belanche, N. Fur N, L. Guzenko, J. Woerle, M.E. Bathen, U. Grossner. MSF, **1092**, 187 (2023). https://doi.org/10.4028/p-0y444y
[18] L. Liszkay, K. Havancsak, M.-F. Barthe, P. Desgardin, L. Henry, Zs. Kajcsos, G. Battistig, E. Szilagyi, V.A. Skuratov. Mater. Sci. Forum, **363**, 123 (2001). https://doi.org/10.4028/www.scientific.net/MSF.363-365.123
[19] V.V. Kozlovski, A.E. Vasil'ev, P.A. Karasev, A.A. Lebedev. Semiconductors, **52**, 310 (2018). https://doi.org/10.1134/S1063782618030132
[20] M.J. Madito, T.T. Hlatshwayo, V.A. Skuratov, C.B. Mtshali, N. Manyala, Z.M. Khumalo. Appl. Surf. Sci., **493**, 1291 (2019). https://doi.org/10.1016/j.apsusc.2019.07.147
[21] A. Gottwald, U. Kroth, E. Kalinina, V. Zabrodskii. Appl. Opt., **57** (28), 8431 (2018). https://doi.org/10.1364/AO.57.008431

Translated by T.Zorina